Available online at www.sciencedirect.com
ScienceDirect
Polymer 48 (2007) 2387–2394
polymer
www.elsevier.com/locate/polymer

# Gel-size dependence of temperature-induced microphase separation in weakly-charged polymer gels

Fumiyoshi Ikkai [a,*], Mitsuhiro Shibayama [b]

[a] L'Oreal Recherche, Nihon L'Oreal K.K., KSP R&D-D637, 3-2-1 Sakado, Takatsu-ku, Kawasaki, Kanagawa 213-0012, Japan
[b] Neutron Science Laboratory, The Institute for Solid State Physics, The University of Tokyo, Tokai, Naka-gun, Ibaraki 319-1106, Japan

Received 2 August 2006; accepted 19 February 2007
Available online 22 February 2007

**Abstract**

The gel-size dependence of microphase separation in weakly-charged gels of *N*-isopropylacrylamide (NIPA) and 1-vinylimidazole (VI) copolymers has been investigated using swelling measurement, small-angle neutron scattering (SANS), and dynamic and static light scattering (DLS/SLS). It is known that weakly-charged polymer gels undergo microphase separation in a poor solvent as a result of competing interactions involving hydrophobic attraction versus electrostatic repulsion. The microphase separation is characterized by a scattering maximum in SANS intensity functions of which Bragg spacing, $\Lambda$, is around 20–30 nm. However, when gel size was reduced to the order of $\Lambda$, no microphase separation was observed. Instead, a typical scattering of isolated spherical particles was clearly observed. On the basis of the experimental evidence, we conclude that microphase separation has its own wavelength independent of gel size, and nanometer-order gels, i.e., nanogels, do not undergo microphase separation.


*Keywords:* Microphase separation; Polymer gel; Scattering

## 1. Introduction

*N*-isopropylacrylamide (NIPA) gels and their ionized derivatives are known to undergo volume phase transition [1–14]. A temperature-induced volume phase transition at $T_{NIPA}$ ($\approx$34 °C) was first reported for a NIPA homopolymer gel by Hirokawa and Tanaka in 1984 [6]. They suggested that the discreteness of the transition was due to the stiffness of the polymer network chains. Tanaka and his coworkers also reported that introducing ionizable groups in the polymer network increased osmotic pressure and expanded the network, resulting in a discontinuous volume transition with a larger volume change of about tens to hundreds times [9,15–18]. Just before the volume phase transition, the ionized NIPA copolymer gels go through an interesting state which is called the microphase separation, where a swollen phase (ionized hydrophilic parts) and a shrunken phase (hydrophobic parts) coexist microscopically in a gel. Starting with Schosseler's work for partially neutralized poly(acrylic acid) gels [19], many experimental demonstrations [3,4,10,13,14] and theoretical explanations [20–24] have clarified the physical origin of the microphase separation and its parameter dependence. Especially pertaining to NIPA/acrylic acid copolymer gels, Shibayama et al. showed the existence of microphase separation in gels using small-angle neutron scattering (SANS) [10,16,25,26]. The SANS profiles showed a broad but clear peak at around 0.02 $Å^{-1}$ of scattering vector, $q$, for temperatures $T > T_{NIPA}$. The peak position, $q_m$, was slightly dependent on the amount of ionized groups, the degree of dissociation, and the ionic strength. The $q$ value at ca. 0.02 $Å^{-1}$ corresponds to a characteristic length of 20–30 nm for microphase separation. Schosseler et al. [14,27] and Shibayama et al. [16,25] analyzed SANS intensity functions of weakly-charged polymer gels by fitting with theoretical functions proposed by Borue–Erukhimovich (BE) [28] and

* Corresponding author. Tel.: +81 44 812 2013; fax: +81 44 812 2033.
*E-mail address:* fikkai@rd.loreal.com (F. Ikkai).

0032-3861/$ - see front matter © 2007 Elsevier Ltd. All rights reserved.
doi:10.1016/j.polymer.2007.02.049

clarified the dependence of the structure factor on the degree of ionization, temperature, and salt concentration. However, since BE theory was originally developed for weakly-charged polymer solution in a poor solvent, the effects of cross-linking density and/or swelling were not included in the theory. Recently, Rabin and Panyukov (RP) theorized comprehensively the microphase separation in weakly-charged polymer gels in a poor solvent [23,29]. RP theory takes account of the conditions of both preparation and observation and solely describes the contribution of frozen concentration fluctuations, i.e., inhomogeneities. Using RP theory, Shibayama and coworkers quantitatively analyzed microphase separation and inhomogeneities of the gels [26,30–32].

However, most of these experiments and analyses on volume phase transition and microphase separation have been carried out on polymer gels having a gel size much larger than the characteristic size of microphase separation, $\Lambda$. Furthermore, a small sum of researches of very small microgel particles had not paid attention to the relationship between volume phase separation and microphase separation [33–35]. The purpose of this study is to understand whether microphase separation depends on the size of the gel and what happens when its size was of the same order as $\Lambda$? We investigated gel-size dependence of microphase separation in weakly-charged polymer gels using swelling measurement, dynamic/static light scattering (DLS/SLS), and SANS. We prepared two types of gels, i.e., (a) bulk gels whose size was higher than μm-order and (b) nanometer-order gel particles, nanogels, and we compared the swelling behavior and SANS profiles of the two types of gels.

## 2. Theory

Here, we briefly describe the theoretical background of microphase separation of weakly-charged gels with the Rabin–Panyukov theory (RP theory) [23]. RP theory properly describes the frozen inhomogeneities in addition to two opposite interactions, i.e., electrostatic (repulsive) and hydrophobic (attractive), on the basis of a mean-field theory of polymer gels [23,29,36]. The theoretical structural factor, $S(q)$, consists of two contributions, one from static inhomogeneities, $C(q)$, and the other one from thermal concentration fluctuations, $G(q)$, where $q$ is the scattering vector. Both $C(q)$ and $G(q)$ are built up with well-defined parameters, i.e., the cross-linking density, CD, the polymer volume fraction (polymer concentration), $\phi$, the degree of ionization, $f$, and temperature, $T$ (or the Flory interaction parameter, $\chi$). Here, we define CD as $\mathrm{CD} = [2C_{\mathrm{crosslinker}}/(C_{\mathrm{polymer}} + 2C_{\mathrm{crosslinker}})]$. Using two sets of parameters, i.e., those at sample preparation time, $\phi_0$, $f_0$, $\chi_0$, in addition to those at observation time, $\phi$, $f$, $\chi$, $S(q)$ is given by Eqs. (1)–(3):

$$S(q) = G(q) + C(q) \tag{1}$$

$$G(q) = \frac{\phi N g(q)}{1 + w(q)g(q)} \tag{2}$$

$$C(q) = \frac{\phi N}{[1 + w(q)g(q)]^2 (1 + Q^2)^2} \times \left[6 + \frac{9}{w_0(q) - 1 + (1/2)Q^2(\phi_0/\phi)^{2/3}\phi_0^{-1/4}}\right] \tag{3}$$

where the subscript 0 means the parameter value at sample preparation time, and $a$, $N$, and $w(q)$ indicate the segment length (8.12 Å for NIPA polymer chains [16,37]), the average degree of polymerization between crosslinks ($N \sim 1/\mathrm{CD}$), and the effective second virial coefficient, respectively. $Q$ ($=aN^{1/2}q$) is the dimensionless wave vector. The function $g(q)$ is given by Eq. (4):

$$g(q) = \frac{1}{Q^2/2 + (4Q^2)^{-1} + 1} + \frac{2(\phi/\phi_0)^{2/3}\phi_0^{1/4}}{(1 + Q^2)^2} \tag{4}$$

The functions of $w(q)$ and $w_0(q)$ are expressed by Eqs. (5) and (6), respectively:

$$w(q) = (1 - 2\chi + \phi)\phi N + \frac{l_B f^2 \phi N^2}{Q^2 + l_B f \phi N} \tag{5}$$

$$w_0(q) = \phi_0^{5/4} N + \frac{l_B f_0^2 \phi_0^{5/4} N^2}{Q^2(\phi_0/\phi)^{2/3} + l_B f_0 \phi_0^{5/4} N} \tag{6}$$

$l_B$ is the dimensionless Bjerrum length given by $l_B = 4\pi L_B/a$, where $L_B$ is the Bjerrum length fixed as 7 Å for aqueous solutions at 25 °C.

## 3. Experimental section

### 3.1. Materials

Weakly-charged nanogels were prepared by heat-induced copolymerization of NIPA, 1-vinylimidazole (VI) (see Fig. 1), and *N*,*N*′-methylenebisacrylamide (BIS) (crosslinker) using ammonium persulfate (APS) (initiator) and sodium dodecylbenzenesulfonate (SDS) (surfactant) [38]. The molar ratio of those components is NIPA/VI/BIS/APS = 360/40/4/4.4 (mM). Degree of ionization is estimated to be 0.1 for full ionization. Nanogels with various sizes were prepared by copolymerization of a 200 mL of aqueous solution containing 400 mM of the monomer and 1 wt% of BIS in a 300 mL round-bottom flask for 4 h at 60 °C with stirring under $N_2$ atmosphere. The size of nanogels was tuned with the SDS concentration and the stirring rate. After polymerization, residual monomers and SDS were removed by dialyzing the polymer for a week

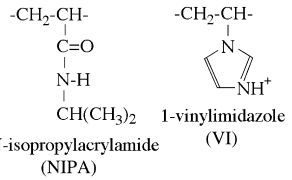


Fig. 1. Chemical structures of *N*-isopropylacrylamide (NIPA) and 1-vinylimidazole (VI).

with 0.1 N HCl and ionized water. After dialysis, the hydrodynamic radii of the nanogel, $R_h$, were measured by dynamic light scattering as described below. For SANS, the nanogels were dried and then immersed in pure $D_2O$ and pH-controlled $D_2O$. Finally, $R_h$ values of prepared nanogels were 309 nm, 164 nm, 79.2 nm, and 57.2 nm at pH 7 and 340 nm, 290 nm, 140 nm, and 80 nm at pH 3. On the other hand, the bulk gels for SANS were prepared in an 8 mm $\phi$ test tube with the same compositions without SDS. The gels were then sieved with a 500 μm filter, washed with a large amount of water, and dried. Then, the dried gels were swollen with $D_2O$ until reaching their equilibrium state. For swelling measurements of bulk gels, cylindrical gels were prepared in 10 μL micropipettes.

### 3.2. Swelling measurement

The diameter of the cylindrical gels was measured under an inverted microscope coupled with a charge capacity device (CCD) camera. During the measurements, the gels were immersed in a water-filled quartz cell under controlled temperature within ±0.1 °C.

### 3.3. DLS/SLS

Dynamic and static light scattering (DLS/SLS) experiments were carried out on a DLS/SLS-5000 (ALV, Co Ltd.) with a 22 mW He–Ne laser (wavelength, $\lambda = 632.8$ nm). Aqueous solutions containing 0.1% of nanogel were adjusted and were put into the test tube (inner diameter, $d = 8$ mm), which was placed in a temperature-controlled decalin bath within an error of ±0.1 °C. In DLS, by monitoring the change of scattered intensity in kHz units for 30 s at a scattering angle of 90°, we obtained a time-averaged intensity correlation function (ICF) and the time-averaged scattered intensity, $\langle I \rangle_T$. ICF is defined by Eq. (7):

$$g^{(2)}(\tau) - 1 = \frac{\langle I(t)I(\tau)\rangle_T}{\langle I(t)\rangle_T^2} - 1 = \left[\int_0^\infty G(\Gamma)\exp(-\Gamma\tau)d\Gamma\right]^2 \quad (7)$$

where $t$ is time and $\tau$ time lag. $\langle\ \rangle_T$ denotes time averaging. $\Gamma$ is the characteristic decay rate. If translation diffusive behavior was assumed, $\Gamma$ would be related to the cooperative diffusion coefficient, $D$ with $\Gamma = Dq^2$. $G(\Gamma)$ is the distribution function of $\Gamma$. The hydrodynamic radius, $R_h$, of the nanogel was obtained with the following equation:

$$R_h = \frac{kT}{6\pi\eta D} \quad (8)$$

where $kT$ denotes Boltzmann energy and $\eta$ solvent viscosity. $D$ was calculated from $\Gamma$ at the point where $G(\Gamma)$ was maximum. The measurements were conducted at temperatures from 20 °C to 70 °C. Here, each measurement was taken after keeping the samples at the desired temperatures for more than 15 min for thermal equilibration.

SLS measurements were carried out at the same set-up as DLS. The radius of gyration, $R_g$, was determined by measuring the excess Rayleigh ratio, $R_{ex}(q)$, at 30°–150° in 5° steps on the basis of Eq. (9) [39]:

$$\frac{KC}{R_{ex}(q)} \cong \frac{1}{M_w}\left(1 + \frac{1}{3}R_g^2q^2\right) + 2A_2C \quad (9)$$

where $M_w$ is the weight averaged molecular weight, $C$ the polymer concentration, and $A_2$ Avogadro's constant. $K$ is the optical constant defined by $4\pi^2n_0^2(\partial n/\partial C)^2/(\lambda_0^4N_A)$with $n_0$, $n$, and $\lambda_0$ being the solvent refractive index, the solution refractive index, and wavelength of light in vacuo.

### 3.4. SANS

Small-angle neutron scattering (SANS) experiments were carried out at a two-dimensional SANS spectrometer (SANS-U) of Institute for Solid State Physics, University of Tokyo, located at Tokai, Japan. The SANS intensity functions were collected at room temperature for 1.5 h and 8 h, respectively, at 2 m and 8 m sample-to-detector distance. Gel samples of 1 wt% in quartz cells with 4-mm optical path were irradiated with a neutron beam having a wavelength of 7.0 Å. The wavelength distribution of the incident neutron beam, $W_\lambda(\lambda)$, is known to be $W_\lambda(\lambda) = 0.1$. The scattered intensity was circularly averaged and rescaled to the absolute intensity scale with a polyethylene secondary standard calibrated for the incoherent scattering from vanadium. The solvent correction for scattered intensity was made using Eq. (10):

$$I(q) = I_{sample}(q) - (1 - \phi_p)I_{D_2O}(q) - I_{incoh}(q) \quad (10)$$

where $I_k(q)$ denotes the observed scattered intensity in absolute scale of the kind k (=sample, $D_2O$, and the incoherent scattering of the NIPA monomer solution) and $\phi_p$ is the volume fraction of the polymer.

## 4. Results and discussion

### 4.1. Swelling behavior of NIPA/VI gels

Fig. 2 shows the temperature dependence of the swelling behavior of NIPA/VI copolymer gels, (a) bulk gels at pH 3 and 7, (b) nanogels at pH 7, and (c) nanogels at pH 3. Note that NIPA/VI copolymer gels are fully ionized at pH 3. As shown in the Fig. 2a, the NIPA homopolymer bulk gel undergoes a volume phase transition at ca. 34 °C ($\approx T_{NIPA}$). On the other hand, introduction of charges, i.e., NIPA gels to NIPA/VI gels, leads to an increase in transition temperature toward a higher temperature (see for example, ca. 50 °C at pH 7). This is due to the electrostatic interaction between the weakly-charged VI groups in the NIPA/VI gels. This transition occurred very sharply at the volume phase transition temperature, $T_{NV}$ ($T_{NV} > T_{NIPA}$) and the volume change was about 30 fold the initial volume. This type of transition has been recognized as one of the characteristic features of weakly-charged polymer gels. A decrease in pH (pH 3) results in no volume change in the temperature range of 20–70 °C. The reason

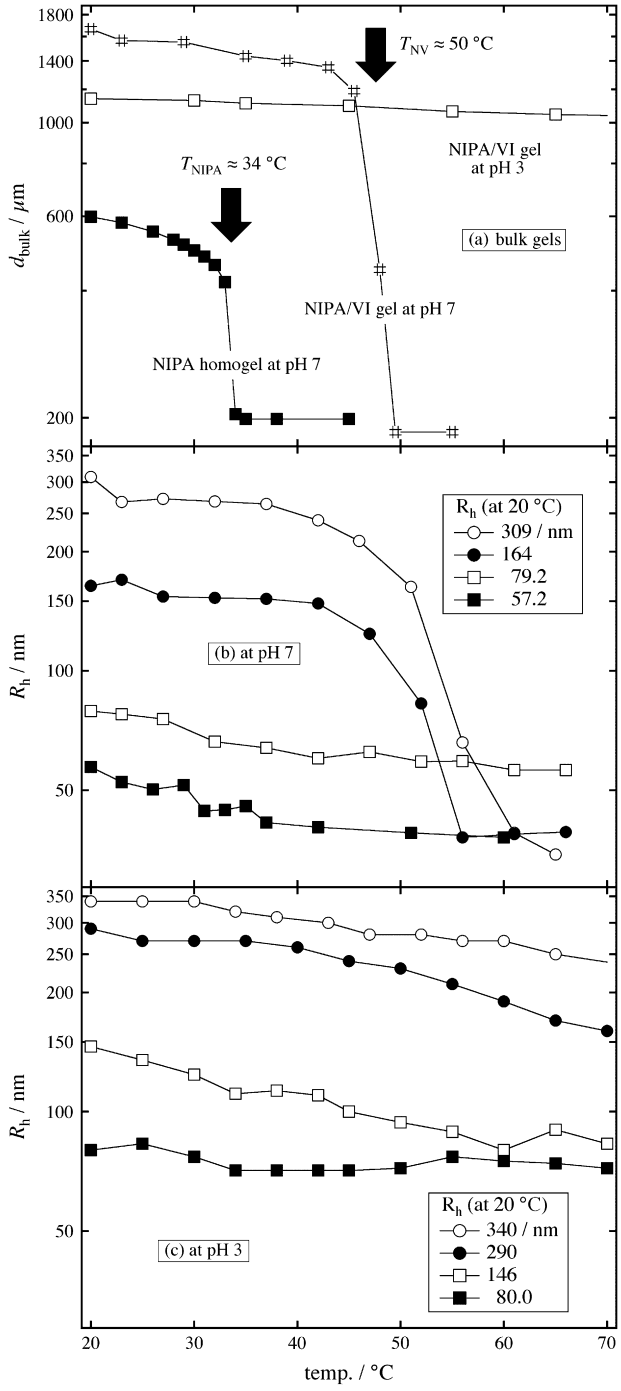


Fig. 2. Temperature dependence of gel sizes for NIPA/VI gels: (a) bulk gels at pH 3 and 7, (b) nanogels at pH 7, and (c) nanogels at pH 3. For bulk gels, the diameter of cylindrical gel, $d_{bulk}$, was measured. For nanogels, the hydrodynamic radius, $R_h$, of the particles was measured by DLS. Thick arrows show the volume phase transition temperature; $T_{NIPA} \approx 34$ °C for NIPA homogel at pH 7 and $T_{NV} \approx 50$ °C for NIPA/VI gel at pH 7.

is that the weakly-charged VI groups are yet too strongly charged at this pH to undergo a volume phase transition in this temperature range. On the other hand, as shown in Fig. 2b, the microphase separation seems to depend on the size of nanogels. The nanogels at pH 7 with $R_h$ of 309 nm and 164 nm at 20 °C also showed volume phase transition at around 50 °C ($\approx T_{NV}$) just like bulk gels at pH 7. However, nanogels at pH 7 with $R_h$ of 79.2 nm and 57.2 nm at 20 °C did not undergo volume phase transition. In Fig. 2c, nanogels at pH 3 with four different $R_h$s at 20 °C gradually shrank with $T$, without accompanying any discrete volume transition, probably due to the same reason as the bulk gel at pH 3 in Fig. 2a.

### 4.2. Dynamic and static light scattering

By applying a simple method of Burchard et al. [40,41], the structure of NIPA/VI nanogels was evaluated. Fig. 3 shows temperature dependence of $R_g/R_h$ of NIPA/VI nanogels with $R_h$ (at 20 °C) = 164 nm and 79.2 nm at pH 7. The former corresponds to nanogels that undergo volume phase transition at $T_{NV}$, and indeed the $R_g/R_h$ increased dramatically near $T_{NV}$ from ca. 0.4 to 0.9 with temperature. This indicated that the NIPA/VI nanogels prepared with $R_h = 164$ nm would have a kind of inhomogeneous core–shell type gel structure below $T_{NV}$ and change to a hard sphere by shrinking of shell parts, because the $R_g/R_h$ value close to 0.775 is predicted for monodispersed hard sphere of constant density [34,40–42]. On the other hand, the NIPA/VI nanogels with $R_h = 79.2$ nm, which corresponds to nanogels that did not undergo volume phase transition, showed a gradual increase of $R_g/R_h$ from ca. 0.7 to 0.9, indicating that the nanogels had a relatively homogeneous gel structure and the non-transition behavior was not related to an imperfect network structure.

### 4.3. Small-angle neutron scattering

To evaluate NIPA/VI nanogel structure in a wider $q$ range, SANS measurements were carried out. For NIPA/acrylic acid (AAc) (=668 mM/32 mM) bulk gels in the previous study [4,16], the microphase separation was readily observed near and beyond the transition temperature. However, in this NIPA/VI (=360 mM/40 mM) bulk gels at pH 7, microphase

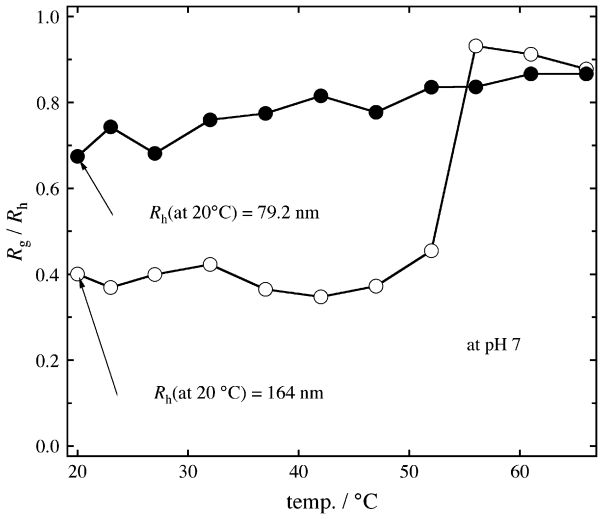


Fig. 3. Temperature dependence of the ratio of $R_g/R_h$ at pH 7 for nanogels with $R_h$ (at 20 °C) = 79.2 nm and 164 nm, where $R_g$ is the radius of gyration obtained by SLS and $R_h$ the hydrodynamic radius obtained by DLS.

separation was observed only at narrow temperature range around 50 °C, following macrophase separation beyond the temperature range. On the other hand, at pH 3, the volume phase transition did not occur because of the strongly charged effect, but microphase separation was observed clearly even at 75 °C as will be reported in Section 4.4. Therefore, we compared microstructure of bulk gel with that of nanogels at pH 3. Fig. 4 shows SANS profiles of NIPA/VI bulk gel and the nanogels ($R_h = 140$ nm at 20 °C) at pH 3 at (a) 20 °C and (b) 75 °C. Fig. 4a shows the SANS profiles of the bulk gel and nanogels at 20 °C. As shown in the figure, the two $I(q)$s are very different in the shape. At 75 °C (Fig. 4b), the difference in the shapes of $I(q)$s becomes even larger. $I(q)$ of the bulk gel has a broad shoulder at $q = 0.02$–$0.04$ Å$^{-1}$, which is similar to the scattering profile observed with NIPA/AAc copolymer gel systems [16,25], indicating the existence of microphase separation with a characteristic length of a few hundreds of Å. On the other hand, the nanogel has characteristic shoulders in $I(q)$s at $q \approx 0.006$ Å$^{-1}$ (20 °C) and at $q \approx 0.01$ Å$^{-1}$ (75 °C).

Fig. 5 shows the SANS functions of NIPA/VI nanogels at pH 3 obtained at various temperatures. It is clearly seen that $I(q)$ increases and the shoulder shifts toward a higher $q$ with increasing $T$. In addition, the slope of $I(q)$ at higher $q$ ($\geq$0.03 Å$^{-1}$) becomes steeper at $T \geq 33$ °C. These behaviors were found to be thermo-reversible. In the following section, we try a curve fitting with theoretical scattering functions in order to analyze these scattering profiles.

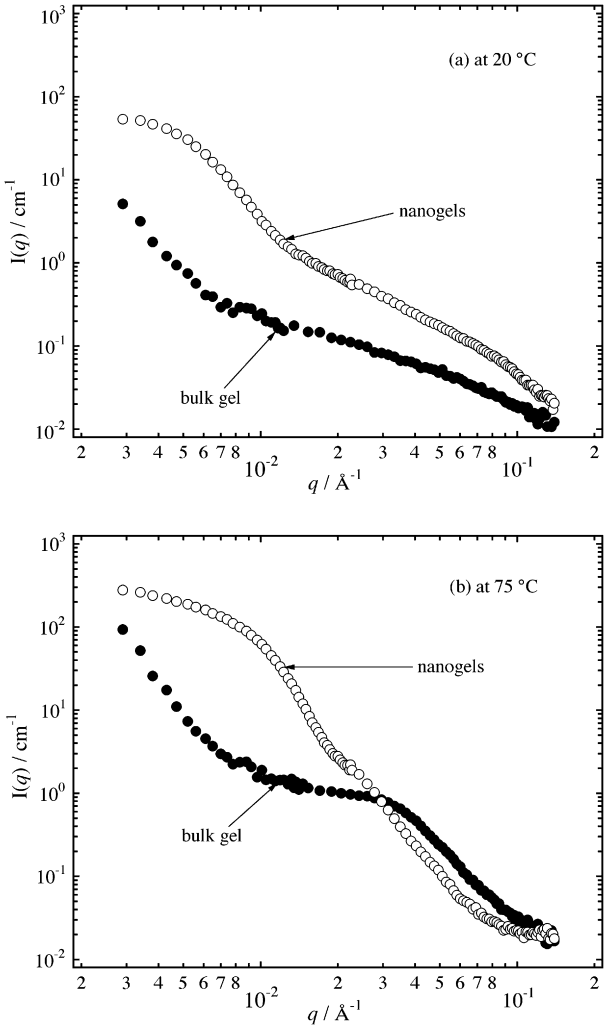


Fig. 4. SANS profiles of NIPA/VI gels, i.e., a bulk gel and nanogels, at (a) 20 °C and (b) 75 °C at pH 3.

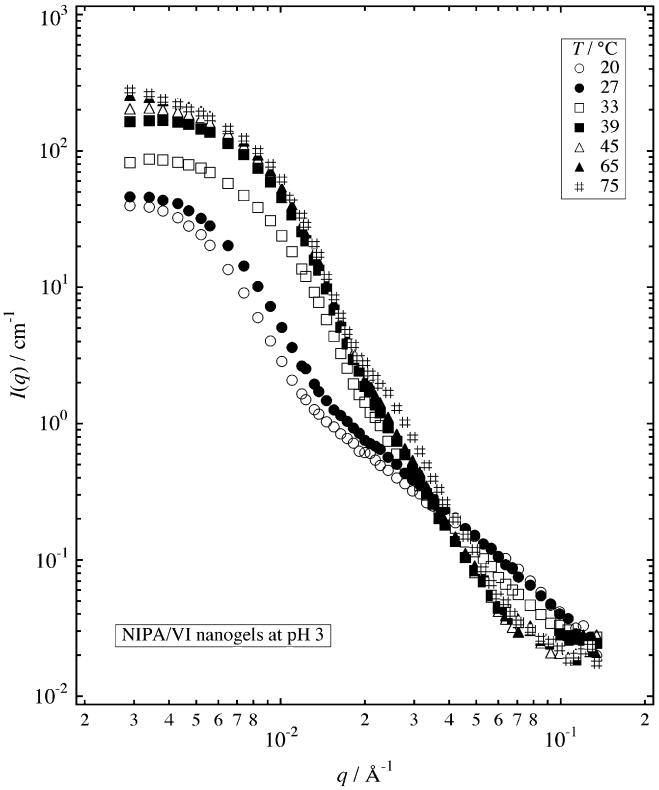


Fig. 5. Temperature dependence of SANS profiles of NIPA/VI nanogels at pH 3.

### 4.4. SANS analyses of nanogels

Fig. 6 shows the SANS profiles of nanogels (pH 3) at 20 °C and 75 °C and the fitting lines (the thick solid lines). At first, both scattering functions at 20 °C and 75 °C are leveled off when $q$ tends toward zero. Because nanogel concentration was 1 wt% and was low enough to be dispersed in the solution, the scattering was solely due to particle scattering and no additional scattering from inter-particle interference was expected. As a matter of fact, the scattering profile at 75 °C were fitted only with an isolated-particle-scattering Eq. (11) as follows [43]:

$$I(q) \sim \frac{d\Sigma}{d\Omega}(q) = \frac{w}{d_p}\left(\rho_{b,p} - \rho_{b,s}\right)^2 \times \frac{\iint W_R(R) W_\lambda(\lambda) V(R) \Phi^2(qR)\, dR d\lambda}{\iint W_R(R) W_\lambda V(R) dR d\lambda} \quad (11)$$

where $w$, $d_p$, $\rho_{b,p}$, $\rho_{b,s}$, and $V(R)$ are the polymer weight fraction, the polymer density, the scattering densities of polymer and solvent, and the volume of the sphere, respectively. The

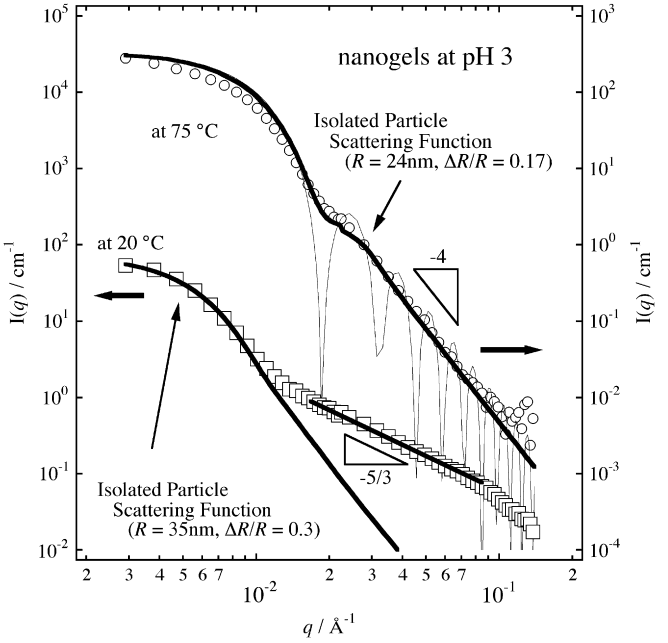


Fig. 6. Curve fitting results for nanogels at 20 °C and 75 °C at pH 3. Open circles and open squares show data points at 20 °C and 75 °C, respectively. Thick solid lines are theoretical fitting curves. Thin solid line corresponds to an isolated mono-sized particle scattering function.

isolated scattering factor of particle, $\Phi(qR)$ is expressed by Eq. (12):

$$\Phi(qR) = \frac{3[\sin(qR) - qR\cos(qR)]}{(qR)^3} \tag{12}$$

The distribution of the particle radius, $W_R(R)$, and the neutron wavelength, $W_\lambda(\lambda)$, was estimated from Eqs. (13) and (14), respectively.

$$W_R(R) \sim \exp\left[-\frac{(R-\overline{R})^2}{2\sigma_R^2}\right] \tag{13}$$

$$W_\lambda(\lambda) \sim \exp\left[-\frac{(\lambda-\overline{\lambda})^2}{2\sigma_\lambda^2}\right] \tag{14}$$

where $\overline{R}$, $\overline{\lambda}$, $\sigma_R$, and $\sigma_\lambda$ denote the averaged $R$, $\lambda$ and the standard deviations of $R$ and $\lambda$, respectively. The particle size and the size distribution at 75 °C were estimated to be 24 nm and $W_R(R) = 0.17$ with $W_\lambda(\lambda) = 0.1$. Furthermore, the profile at the higher $q$ range showed a slope of −4, meaning that the system is a two phase system with a sharp boundary. The fact that $I(q)$ can be fitted only with the isolated-particle-scattering function indicates that microphase separation observed in bulk gels did not occur in nanogels. Fernandez-Barbero et al. analyzed SANS profiles of nanogels by using a combination of fractal equations and concluded that the nanogel structure could be recognized by a hard core−shell model with clear surfaces [35]. However, the SANS profiles seem to have a broad size distribution and nanogel size larger than ours resulting in the appearance of fractal nature.

On the other hand, the SANS profile at 20 °C can be fitted with an isolated-particle-scattering function at lower $q$ range. From the fitting at lower $q$, the particle size at 20 °C was estimated to be 35 nm with $W_R(R) = 0.3$, meaning that the nanogels swelled at 20 °C with a ratio of about 1.5. At higher $q$ range, corresponding to the spatial range of a swollen gel with an ambiguous surface, the SANS probably catches information inside the nanogels. The slope of −5/3 at higher $q$ range may indicate a random coil-type structure in a good solvent inside a nanogel particle.

### 4.5. SANS analyses of bulk gels

Fig. 7 shows SANS profiles of bulk gels at 20 °C and 75 °C. The thick solid lines are theoretical functions. It is noteworthy that the shapes of $I(q)$s of bulk gel at 75 °C and 20 °C are very different from those of nanogel, particularly in the lower $q$ region. The $I(q)$ of bulk gel exhibits a straight upturn when $q$ tends toward zero, while that of nanogel has a broad shoulder. At 20 °C, the $I(q)$ of bulk gel at the high $q$ range fits well with the Ornstein−Zernike (OZ) equation, which expresses a solution-like concentration fluctuations. The fitting equation is given by Eq. (15) [44]:

$$I(q) = \frac{I(0)}{1+\xi^2 q^2} \tag{15}$$

where $\xi$ denotes a correlation length of the concentration fluctuations. In this case, the value of $\xi$ was estimated to be 24 Å. The steep increase in scattered intensity at lower $q$ range probably results from large-scale structural inhomogeneities in the gel network formed at the preparation stage, which has been

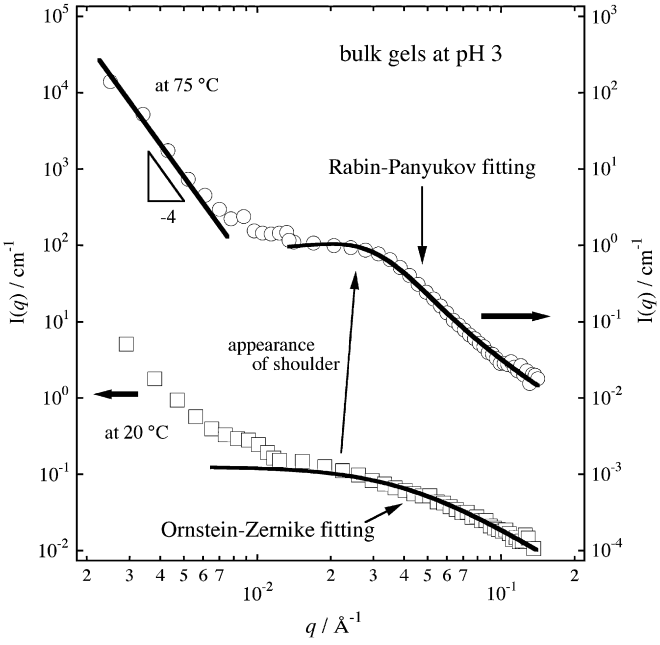


Fig. 7. Theoretical fitting results for bulk gels at 20 °C and 75 °C at pH 3. Open circles and open squares show data points at 20 °C and 75 °C, respectively. Thick solid lines are theoretical fitting curves.

discussed in many papers [35,45–49]. At 75 °C, on the other hand, the $q$ dependence of SANS profile at high $q$ range could not be expressed by the OZ equation, where a clear shoulder (or broad peak) appeared. Appearance of such broad peak is observed for charged polymer system in a poor solvent. In partially-ionized NIPA gels, it is well known that the $I(q)$ in a poor solvent has a distinct scattering maximum as a result of microphase separation, though $I(q)$ in a good solvent is similar to that of non-charged polymer gels expressed by OZ equation. In order to carry out curve fitting, we used the Rabin–Panyukov (RP) theory [23], assuming that the shoulder originates from weakly-charge-induced microphase separation in poor solvent conditions. As shown in the figure, a fitting result with $\chi = 0.89$ and $N = 51$ looks quite satisfactory, where we used the following parameters: the polymer volume fraction, $\phi = \phi_0 = 0.04$, and the degree of ionization, $f = f_0 = 0.090$. These values are reasonable even in comparison with the experimental ones, i.e., $\phi_0 = 0.04$ (the total concentration of NIPA and NV was 400 mM) and $f_0 = 0.1$ for full ionization. The broad shoulder appeared at the high $T$ is assigned to a peak originating from microphase separation as is well known for weakly-charged polymer gels in poor solvent.

### 4.6. Interpretation of microphase separation

In this section, we discuss the gel-size dependence of the microphase separation. Fig. 8 is an illustration showing the relationship between microphase separation and the size of gel, i.e., bulk gel (upper) versus nanogel (lower). A bulk gel having the size $d_{bulk}$ is homogeneous at a temperature below the transition (Fig. 8a). However, by increasing $T$, strong concentration fluctuations appear due to competition between hydrophobic and electrostatic interactions. This leads to a microphase separation with the wavelength of the concentration fluctuations, $\Lambda$, as schematically depicted in Fig. 8b. The graphs under the figures show the density fluctuation with position $r$, $\rho(r)$. On the other hand, a nanogel with the same order of $\Lambda$ shrinks without undergoing microphase separation with increasing $T$. This phenomenon is explained as follows: the wavelength of the concentration fluctuations is a function of the degree of ionization, $f$, and the $\chi$ parameter, etc., as discussed with RP theory, but it is expected to be independent of gel size. Since the gel size of a bulk gel, $d_{bulk}$, is much larger than $\Lambda$, the gel has enough space for microphase separation to occur. However, when gel size is of the order of $\Lambda$, concentration fluctuations generated by the competition of hydrophobic and electrostatic interactions are deteriorated by wave-propagation through the gel surface. As a result, the effect of particle surface is not to be neglected in the case of nanogels with a few tens of nanometer size. Surface tension may also suppress microphase separation. Hence, as shown in Fig. 8d, a nanogel with a diameter of $d_{nanogel}$ (close to $\Lambda$) does not undergo a microphase separation when it shrinks with $T$. That is, even if the temperature is close to that of volume transition, the SANS profile never shows a microphase separation peak but is described only by the isolated-particle-scattering. Meanwhile, the small volume of the nanogel may make it easier for water to enter and exit from the gel network, leading to a quick release of concentration fluctuations of the wavelength of $\Lambda$. In other words, strong concentration fluctuations created by the antagonistic interactions of the hydrophobic contraction and Donnan potential repulsion is released by the presence of the gel surface. This may indicate the importance of the gel surface for designing gel microstructure and the kinetic response of swelling/shrinking.

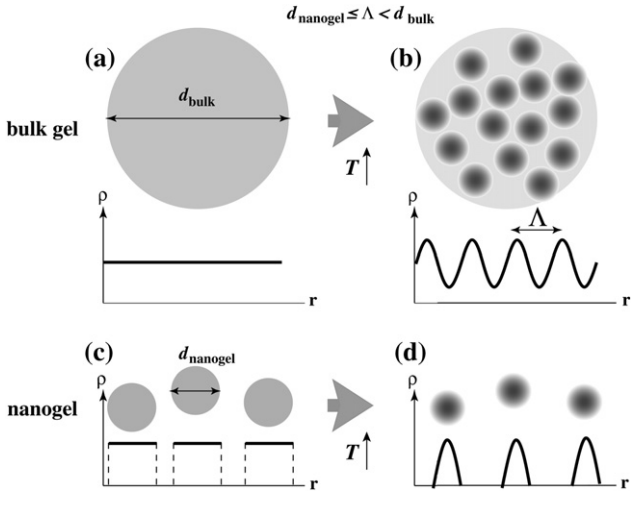


Fig. 8. Illustration of the relationship between microphase separation and the gel size of a bulk gel (upper) and a nanogel (lower); (a) and (b) show a bulk gel having the size of $d_{bulk}$ and the temperature-induced microphase separation with the wavelength of the concentration fluctuations of $\Lambda$, respectively. (c) and (d) show nanogel with a diameter of $d_{nanogel}$, where $d_{nanogel}$ is close to $\Lambda$. The graphs under the figures show the density ($\rho$) fluctuations.

## 5. Conclusions

We investigated the gel-size dependence of microphase separation by using temperature-dependent swelling behavior measurement, dynamic/static light scattering, and small-angle neutron scattering. In DLS/SLS measurements at pH 7, the swelling behavior depended on nanogel size, i.e., nanogels with $R_h$ larger than 164 nm showed volume phase transition, just as the bulk gels. On the other hand, those smaller than 79.2 nm did not undergo volume transition. At pH 3, both the bulk gel and the nanogels showed a similar swelling behavior, i.e., both gels gradually shrank with $T$. However, the SANS profiles at pH 3 were completely different, particularly near the transition temperature. In the case of bulk gel, the SANS profiles showed a broad peak at higher $T$, and were well represented by the Rabin–Panyukov theory. The long spacing of phase separation was estimated to be a few tens of nanometers. On the other hand, in the case of nanogel whose size was in the range of a few tens of nanometers, the SANS profiles were reproduced only by isolated-particle scattering function, indicating the absence of microphase separation. These differences are interpreted through the existence or absence of necessary length scale to form microphase separation, i.e., bulk gels have scale large enough to produce microphase separated structure with the size of a few tens of nanometers, but nanogels do not.

## Acknowledgements

We acknowledge to Dr. Takeshi Karino for his experimental support of SANS measurements at Tokai. The authors would like to thank Mr. Satoshi Okabe for his help to the computer programming.

## References

[1] Tanaka T. Polymer 1979;20:1404.
[2] Tanaka T, Sato E, Hirokawa Y, Hirotsu S, Peetermans J. Phys Rev Lett 1985;55(22):2455–8.
[3] Shibayama M, Tanaka T, Han CC. J Chem Phys 1992;97:6829–41.
[4] Shibayama M, Tanaka T. Adv Polym Sci 1993;109:1–62.
[5] Annaka M, Tanaka T. Phase Transitions 1994;47:143.
[6] Hirokawa Y, Tanaka T. J Chem Phys 1984;81:6379.
[7] Hirose Y, Amiya T, Hirokawa Y, Tanaka T. Macromolecules 1987;20(6): 1342–4.
[8] Hirose H, Shibayama M. Macromolecules 1998;31:5336–42.
[9] Hirotsu S, Hirokawa Y, Tanaka T. J Chem Phys 1987;87:1392.
[10] Nasimova IR, Karino T, Okabe S, Nagao M, Shibayama M. J Chem Phys 2004;121(19):9708–15.
[11] Sato-Matsuo E, Tanaka T. J Chem Phys 1988;89:1695.
[12] Wu C, Zhou S, Au-Yeng SCF, Jiang S. Die Angew Makromol Chem 1996;240:123–36.
[13] Ikkai F, Shibayama M. J Polym Sci Part B Polym Phys 2005;43:617–28.
[14] Schosseler F, Skouri R, Munch JP, Candau SJ. J Phys II 1994;4:1221–39.
[15] Tanaka T. Physica 1986;140A:261.
[16] Shibayama M, Tanaka T, Han CC. J Chem Phys 1992;97:6842–54.
[17] Annaka M, Tanaka T. Nature 1992;355:430–2.
[18] Takeoka Y, Berker AN, Du R, Enoki T, Grosberg AY, Kardar M, et al. Phys Rev Lett 1999;82:4863–5.
[19] Schosseler F, Ilmain F, Candau SJ. Macromolecules 1991;24:225–34.
[20] Onuki A. Adv Polym Sci 1993;109:63.
[21] Panyukov S, Rabin Y. Macromolecules 1996;29:8530.
[22] Sasaki S, Maeda H. Phys Rev E 1996;54:2761.
[23] Rabin Y, Panyukov S. Macromolecules 1997;30(2):301–12.
[24] Shiwa Y. Eur Phys J B 1998;1:345–52.
[25] Shibayama M, Ikkai F, Inamoto S, Nomura S, Han CC. J Chem Phys 1996;105:4358–66.
[26] Shibayama M, Kawakubo K, Ikkai F, Imai M. Macromolecules 1998; 31(8):2586–92.
[27] Moussaid A, Schosseler F, Munch JP, Candau SJ. J Phys II France 1993; 3:573.
[28] Borue V, Erukhimovich I. Macromolecules 1988;21(11):3240–9.
[29] Panyukov S, Rabin Y. Phys Rep 1996;269:1–132.
[30] Ikkai F, Shibayama M. Phys Rev E 1997;56(1):R51–4.
[31] Ikkai F, Shibayama M, Han CC. Macromolecules 1998;31:3275.
[32] Shibayama M, Ikkai F, Shiwa Y, Rabin Y. J Chem Phys 1997;107(13): 5227–35.
[33] Saunders BR. Langmuir 2004;20(10):3925–32.
[34] Arleth L, Xia X, Hjelm RP, Wu J, Hu Z. J Polym Sci Part B Polym Phys 2005;43:849–60.
[35] Fernandez-Barbero A, Fernandez-Nieves A, Grillo I, Lopez-Cabarcos E. Phys Rev E 2002;66(5):051803.
[36] Panyukov S, Rabin Y. Macromolecules 1996;29:7960.
[37] Kubota K, Fujishige S, Ando I. Polym J 1990;22:15.
[38] Ito S, Ogawa K, Suzuki H, Wang B, Yoshida R, Kokufuta E. Langmuir 1999;15(12):4289–94.
[39] Chu B. Laser light scattering. Academic Press; 1991.
[40] Schmidt M, Nerger D, Burchard W. Polymer 1979;20:582–8.
[41] Burchard W. Adv Polym Sci 1983;48:1.
[42] Boyko V, Richter S, Grillo I, Geissler E. Macromolecules 2005;38(12): 5266–70.
[43] Okabe S, Sugihara S, Aoshima S, Shibayama M. Macromolecules 2002; 35:8139–46.
[44] de Gennes PG. Scaling concepts in polymer physics. Ithaca: Cornell University; 1979.
[45] Hecht AM, Duplessix R, Geissler E. Macromolecules 1985;18: 2167.
[46] Mendes E, Girard B, Picot C, Buzier M, Boue F, Bastide J. Macromolecules 1993;26:6873.
[47] Rouf-George C, Munch JP, Beinert G, Isel F, Pouchelon A, Palierne JF, et al. Polym Gels Networks 1996;4:435.
[48] Horkay F, Hecht A-M, Grillo I, Basser PJ, Geissler E. J Chem Phys 2002; 117(20):9103–6.
[49] Takata S, Norisuye T, Shibayama M. Macromolecules 2002;35(12): 4779–84.